View Online / Journal Homepage / Table of Contents for this issue
Dynamic Article Links

Soft Matter

Cite this: *Soft Matter*, 2012, **8**, 7610

www.rsc.org/softmatter

PAPER

Directional interactions in semiflexible single-chain polymer folding†

Pablo Englebienne,[ab] Peter A. J. Hilbers,[ab] E. W. Meijer,[b] Tom F. A. De Greef*[ab] and Albert J. Markvoort*[ab]

Received 10th April 2012, Accepted 8th June 2012
DOI: 10.1039/c2sm25832c

Downloaded by TECHNISCHE UNIVERSITEIT EINDHOVEN on 24 August 2012
Published on 22 June 2012 on http://pubs.rsc.org | doi:10.1039/C2SM25832C

Precise control over folded conformations of synthetic polymers is highly desirable in the development of functional nanomaterials for diverse applications. Introducing monomers capable of strong intramolecular hydrogen bonding is a promising route to achieve this control. In the present work we report the use of Wang–Landau Monte Carlo simulations of coarse-grained copolymers to explore the design parameters of these systems on their pathway to collapse. The highly directional nature of hydrogen-bonded supramolecular interactions is modelled by a directional non-bonded potential while a harmonic bending potential is used to take into account the flexibility of the polymer chain, thus making it possible to look at the interplay of both factors. The introduction of directional interactions in the copolymer chain leads to a sharper coil-globule collapse when compared to homopolymers composed of isotropic interacting beads only. Simultaneously, some of the stiffness-dependent structural properties become exacerbated when directional beads are present. Finally, from the heat capacity profiles for the different chain stiffness values we are able to distinguish the prevalence of the collapse of the backbone for highly flexible chains, while as chain stiffness increases folding of the co-polymer due to the directional interactions becomes the dominant feature.

Introduction

The combination of supramolecular chemistry and the continuous advancement in precision polymer synthesis[1–6] has paved the way to the engineering of nanoscopically ordered materials that can respond to various types of stimuli.[7–14] Applications of such ordered self-assembled materials include nanodevices for personalized medicine,[15,16] catalysis in water,[17] semiconductor integrated circuit design[18] and subnanometer porous films for separation processes.[19] The range of diverse applications of these materials demand a precise knowledge of the interplay between the various non-covalent interactions and the resulting nanoscale architecture. Generic coarse-grained models have played an important conceptual role in this respect as they can yield detailed structural information by systematically exploring the design space of supramolecular ordered materials.[20–27]

Inspired by the high precision by which sequence-defined biomolecules such as proteins fold into ordered three-dimensional conformations, we[17,28–30] and others[31–36] have used recent advancements in precision polymer synthesis to endow synthetic macromolecules with the ability to adopt ordered three-dimensional conformations. For example, Hawker and co-workers,[31,33] as well as Lutz and co-workers[34] and Murray and Fulton,[36] elegantly described the use of intramolecular covalent reactions as a means to stabilize the collapsed conformations of copolymers. Such covalent bridges also play an important role in the stabilization of the secondary and tertiary structures of proteins; however, it has been argued that they do not play a major role in the folding process itself.[37] Non-covalent interactions such as hydrogen-bonds, salt bridges and hydrophobic interactions, on the other hand, play a decisive role in the transition from a disordered polypeptide chain into its unique three-dimensional structure.[37] We have recently explored this strategy and shown that copolymers endowed with monomers carrying strong directional hydrogen-bonding motifs indeed collapse into folded, ordered conformations in a variety of solvents.[17,28–30] In order to rationally control the architectures of such non-covalently structured, single-chain polymeric nanoparticles, suitably designed coarse-grained models may be employed to assist in exploring the very large design space of the copolymers. Herein we show that by employing a coarse-grained copolymer model that takes into account directional interactions representing the effect of hydrogen-bonding, it is indeed possible to identify different folding characteristics.

Coarse-grained lattice and off-lattice models have been extensively used to gain insight into the coil-globule collapse transition of polymers.[38–42] For example, coarse-grained simulations of flexible homopolymers have shown how hydrogen-bonding[43,44] and hydrophobicity[45] can significantly influence the

[a]*Computational Biology group, Department of Biomedical Engineering, Eindhoven University of Technology, Eindhoven, The Netherlands. E-mail: a.j.markvoort@tue.nl; t.f.a.d.greef@tue.nl; Fax: +31 40 247 2740; Tel: +31 40 247 2661; +31 40 247 4427*
[b]*Institute for Complex Molecular Systems, Eindhoven University of Technology, Eindhoven, The Netherlands*

† Electronic supplementary information (ESI) available: Expanded figures for structural property histograms (S1), contact maps (S2) and representative structures (S3). See DOI: 10.1039/c2sm25832c

This journal is © The Royal Society of Chemistry 2012

Published on 22 June 2012 on http://pubs.rsc.org | doi:10.1039/C2SM25832C
Downloaded by TECHNISCHE UNIVERSITEIT EINDHOVEN on 24 August 2012

collapse transition leading to markedly different polymorphic transitions and the appearance of ordered globular conformations in the case of directional hydrogen-bonding. The level of structural complexity considerably increases when AB type copolymers are considered. In such a case the number of B-type monomers and the information content of the sequence directly influence the thermodynamic stability and structural characteristics of the globular state.[46,47] Theoretical work on copolymers with hydrophilic/hydrophobic[46,48] and hydrophobic/charged[49,50] monomers has indeed revealed a much richer behaviour as exemplified by the appearance of ordered structures such as hairpins,[49] and the emergence of a sharp folding funnel that promotes thermodynamic stability and kinetic accessibility during polymer collapse.[51]

In this paper we present detailed off-lattice Monte Carlo (MC) simulations of a coarse-grained bead spring model consisting of two types of beads either having an isotropic or an orientation-dependent potential. This orientation-dependent two-body potential represents the directional effect of hydrogen-bonding[52] as it occurs during the collapse transition of single-chain polymeric nanoparticles.[28,29] Wang–Landau sampling[53,54] is used to perform temperature-independent sampling of the possible states of the system, and overcomes problems arising when sampling across a phase transition. We explore the design space of regular copolymers by studying the influence of chain microstructure and chain stiffness on the pathway to collapse. Our results show that the introduction of a directional interaction leads to a sharper coil-globule collapse transition that is distinct from the collapse of the polymer backbone consisting only of isotropic beads.

Method

Model

Copolymers are modelled as N beads of radius $\sigma = 0.35$ connected by $N - 1$ anharmonic springs through a finite extensible nonlinear elastic (FENE) stretching potential[55]

$$V_{\mathrm{FENE}}(r) = -\frac{k}{2} l_0^2 \log\left(1 - \left(\frac{r - l_{\max}}{l_0}\right)^2\right), \quad (1)$$

where r is the separation of the beads, $k = 40$ is a spring constant, $l_0 = 0.70$ is the optimal separation, and $l_{\max} = 0.30$ is the maximum allowed bond stretching.[56] Nonbonded interactions are considered between all monomers separated by at least three bonds. The polymer chain consists of N_{A} beads of type A (backbone monomers) and N_{B} beads of type B (sticky bits). The nonbonded interactions between two A beads, or one A bead and one B bead are modelled *via* a shifted-truncated Lennard-Jones 12-6 (LJ126) potential:

$$V_{\mathrm{LJ126}}(r) = \begin{cases} 4\varepsilon\left[\left(\frac{\sigma}{r}\right)^{12} - \left(\frac{\sigma}{r}\right)^{6}\right] - V(r_c) & \text{if } r < r_c \\ 0 & \text{if } r \geq r_c \end{cases} \quad (2)$$

where r_c is the non-bonded cutoff radius, taken as 2.5σ, and $\varepsilon = 1$. Two B beads interact either *via* a LJ126 potential (isotropic interacting beads) or a modified version (LJA2) introducing a directional preference (directional interacting beads).[57] For this,

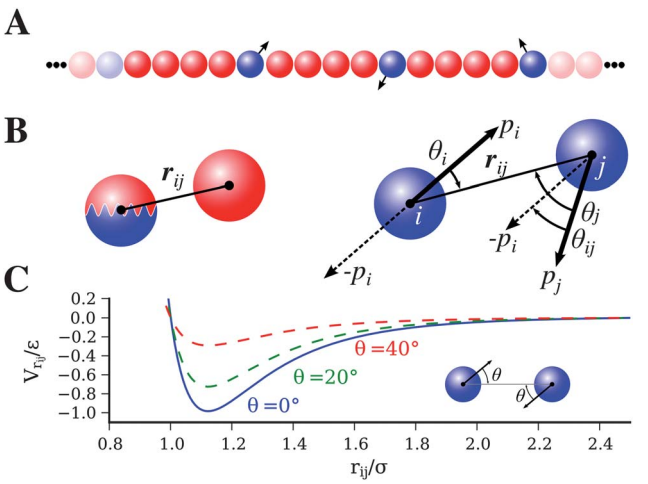

Fig. 1 (A) Schematic of the coarse-grained copolymer sequence with backbone monomers (red, type A) containing one directional bead (blue, type B) as every fifth bead. (B) Non-bonded interactions; left: isotropic LJ126 potential (eqn (2)) involving at least one A-type particle, right: LJA2 directional potential (eqn (3)) between directional sticky bits. (C) Values of the LJA2 potential with parameters: $\theta_i = \theta_j = \theta$, $\theta_{ij} = 0$ and $w = 0.2$.

each particle contains a vector $\boldsymbol{p}_i$ (see Fig. 1) specifying a direction, and the angular dependence is given by an exponential factor:

$$V_{\mathrm{LJA2}}(r, \theta_i, \theta_j, \theta_{ij}) = V_{\mathrm{LJ126}}(r) \times \exp\left(-\frac{\theta_i^2 + \theta_j^2 + \theta_{ij}^2}{4w^2}\right) \quad (3)$$

where the angles θ_i, θ_j and θ_{ij} are depicted in Fig. 1, and $w = 0.2$ is a parameter defining the strength of the directionality; the potential is also shifted and truncated at $r = r_c$. Note that in contrast with the potential used by Bolhuis and co-workers, this potential favours the formation of dimers rather than one-dimensional aggregates. To account for the stronger directional interactions, the parameter ε corresponding to the directional potential is set to 20 times the value of the isotropic potential well depth.

The flexibility of the polymer chain is accounted for by the introduction of a harmonic bending potential involving any three bonded beads:

$$V_{\mathrm{bend}}(\theta_{ijk}) = k_{\mathrm{bend}}(\theta_{ijk} - \theta_0)^2, \quad (4)$$

where θ_{ijk} is the angle between three adjacent beads. We considered six levels of flexibility by varying the value of the bending constant: $k_{\mathrm{bend}} = \{0, 1, 2, 3, 5, 10\}$. In all cases, the reference state was a fully extended polymer, *i.e.*, $\theta_0 = 180°$.

Wang–Landau Monte Carlo simulations

We use the Wang–Landau Monte Carlo sampling scheme[53,54] to get a thorough sampling of the conformations of the polymer chain and to estimate the density of states (DoS) of the system, $g(E)$. The original Wang–Landau sampling consists of a random walk in energy space, where a trial move is accepted with a probability equal to the ratio of the density of states at the initial and final energy values, *i.e.*, $P(E_1 \rightarrow E_2) = \min(1, g(E_1)/g(E_2))$. The estimation of the DoS begins with a flat $g(E)$, which is

Published on 22 June 2012 on http://pubs.rsc.org | doi:10.1039/C2SM25832C
Downloaded by TECHNISCHE UNIVERSITEIT EINDHOVEN on 24 August 2012

multiplied by an update factor f every time a configuration with a given energy is visited. During this process, a histogram of visited energies is kept; once all energy states are sampled and the histogram is "flat" enough (*i.e.*, all energy levels are visited a similar amount of times), the update factor is reduced and the histogram is reset to zero. Initially, the Wang–Landau algorithm was developed and applied to the two-dimensional Ising model, where the energy levels are defined *a priori*. An extension of the algorithm to off-lattice systems is achieved by defining an energy window and splitting it into several bins;[58,59] however, this brings up the issue of having to define the range of energies to sample. As mentioned by Parsons and Williams,[38] the minimum energy to be sampled must be above the global minimum of the system to prevent the simulation from taking prohibitively long CPU time. In order to speed up convergence of the off lattice simulations, we used the modification of the original WL algorithm as proposed by Swetnam and Allen.[60] In this scheme, the update factor is calculated at each sweep from the instantaneous value of the *flatness* of the sampling histogram.

Starting conformations

An initial conformation for the polymer chain is generated by growing a chain with the specified sequence in the centre of a box large enough to make sure that the polymer does not interact with its periodic image. As adjacent particles are placed in a random relative orientation, the chain is relaxed by performing 1000 iterations of a Metropolis Monte Carlo simulation[61] to obtain a configuration with an energy value within the defined energy window.

Monte Carlo trial moves

A hybrid movement algorithm is used in which at each iteration a trial move is selected at random from a pool of possible moves, each having a specific weight. We considered trial moves effecting local changes on the chain, such as single bead translation and rotation, bond stretching and crankshaft moves; other moves involved larger, more global changes: pivot, bond rotation and reptation moves. In a single bead translation, a monomer chosen at random is translated by a small amount in a random direction. In-place rotation of beads is attempted only in the case of directional beads (*i.e.*, with LJA2 non-bonded potential). In a crankshaft move,[62] the portion of a chain between two non-bonded monomers (separated by 1–6 bonds) is rotated by a random angle. In a pivot move,[63] a monomer is randomly selected and the connected chain on one side of the polymer is rotated around a random axis. In a reptation (also known as slithering snake) move,[64] a fragment from either end of the chain is removed and reattached on the opposite end, preserving the sequence of bead types in the process.

Structural parameters

Due to the large number of conformations generated (in the order of 10^{12} per simulation) storing all of them would be space and I/O prohibitive, and taking occasional snapshots would be hardly representative, by the nature of the algorithm. Instead, the distributions of the structural parameters of the polymer chain are monitored for every conformation visited during the simulation to get estimates of the *size* and *shape* of the polymer at every energy value evaluated. We thus calculate the end-to-end distance R_e, radius of gyration R_g, the core density (the number of monomers inside a sphere of radius 2.5σ of the centre of mass of the chain) CD, and the asphericity A:[65]

$$A = \frac{\left(L_1^2 - L_2^2\right)^2 + \left(L_2^2 - L_3^2\right)^2 + \left(L_3^2 - L_1^2\right)^2}{2R_g^4}, \quad (5)$$

involving the principal moments of inertia of the chain L_1, L_2 and L_3. Upon each trial move, the structural parameters are calculated and the corresponding histogram of each structural property at the corresponding energy bin is updated.

Analysis

As Wang–Landau MC simulations are temperature-independent, the DoS obtained from the simulation can be used to construct canonical distributions at any temperature:

$$P(E, T) = g(E)\exp\left(\frac{-E}{k_B T}\right). \quad (6)$$

with an accurate sampling of all energy levels, it is possible to have access to the partition function Z of the system

$$Z(T) = \sum_E g(E)\exp\left(\frac{-E}{k_B T}\right), \quad (7)$$

which in turn allows the determination of all the thermodynamic properties of the system. Following the same principle, the histograms of any descriptor sampled as a function of energy can be transformed to a function of temperature:

$$A(T) = \sum_E A(E)\ g(E)\ \exp\left(\frac{-E}{k_B T}\right). \quad (8)$$

In particular, the heat capacity as a function of temperature can be obtained from the fluctuations of the internal energy of the system:

$$\begin{aligned} U(T) &= \sum_E E\ g(E)\ \exp\left(\frac{-E}{k_B T}\right) \\ C_V(T) &= \frac{\langle U^2\rangle - \langle U\rangle^2}{T^2}. \end{aligned} \quad (9)$$

Contact maps

The existence of contacts between selected beads (*e.g.*, among directional B-type beads) is assessed during the simulation. For each visited conformation, we consider that a contact between a pair exists if the $E_{\text{nonbonded}} < -0.5\varepsilon$. In this way, a $N_B \times N_B$ table is collected for each trial conformation, yielding a two-dimensional histogram at the end of the simulation that can be represented as a heatmap of the probability of finding a contact between the selected beads in the copolymer chain.

Representative structures

Once the DoS of a system is obtained, histograms of structural parameters are analysed (Fig. 2) to extract structural descriptors

 This journal is © The Royal Society of Chemistry 2012

Downloaded by TECHNISCHE UNIVERSITEIT EINDHOVEN on 24 August 2012
Published on 22 June 2012 on http://pubs.rsc.org | doi:10.1039/C2SM25832C

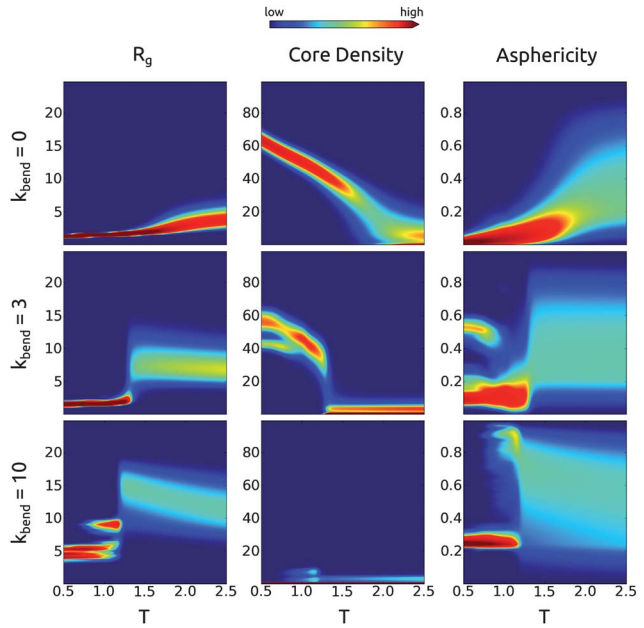

Fig. 2 Distributions of various structural properties of AAAAB type copolymer chains as a function of reduced temperature for selected values of the bending constant (k_{bend}). The scale bar represents the probability of finding a given value of a property at a certain temperature. Distributions for other values of k_{bend} are given in S1A†.

of the polymer chain at specific temperatures. A second simulation is then run, using the best representative values of the structural parameters and the energy at those specific temperatures as a query for all generated conformations. Every conformation generated is scored against each of the parameter sets, and fitness is calculated as

$$\text{Error} = \sum_{i \in \text{ parameters}} f_i(x_i - x_{0,i})^2, \qquad (10)$$

where $x_{0,i}$ are the values for the query parameters, x_i are the actual values of the parameters in the structure, and f_i are scaling factors. The latter are used to weigh the individual error contributions for each parameter based on their expected range. The sum is performed over all the structural parameters discussed above. For each parameter set, the conformation with the lowest error (*i.e.*, closest to the query descriptors) is stored.

Parameters

A regular copolymer sequence AAAAB is compared to a homopolymer with all A-type beads. This ratio of B beads in the chain roughly corresponds to the fraction of monomers with supramolecular moieties experimentally studied in ref. 28 and 29. The non-bonded interactions involving A-type beads have $\varepsilon_{AA} = \varepsilon_{AB} = 1$. The directional potential (LJA2) between B-type beads has $\varepsilon_{BB} = 20$. The energy window to be sampled by the Wang–Landau algorithm is determined by a short Wang–Landau run (5×10^6 MC iterations) with a wide energy range; the minimum energy is set as the lowest energy that was regularly sampled, and the maximum is set so that the energy window spans 1000ε. The Wang–Landau simulations are performed for up to 10^{10} iterations, or whenever the f update factor became lower than 10^{-7}. Each MC iteration consists of 125 trial moves, randomly selected from a pool with a probability distribution 100 : 20 : 1 : 1 : 1 : 1 : 1 of atom translation, atom rotation, rotation around a bond, crankshaft, pivot, reptation and bond stretching, respectively. This combination provides a good balance of computational cost and thorough sampling of the different degrees of freedom of the system.

Results and discussion

Wang–Landau simulations were performed on AAAAB type copolymers of length 100 with varying stiffness, modelled by the value of the harmonic bending constant k_{bend}. The sampled energy window is empirically determined for each copolymer system from a short Wang–Landau run, and the number of energy bins is adjusted so that there are about 1000 energy levels of width 1 (in units of ε, the potential well of the nonbonded interaction between A-type beads). During simulations, a histogram of the values of the different structural parameters is kept for each energy bin. Conversion of the sampled energies to reduced temperatures using eqn (8) results in histograms of the structural properties of the copolymeric chains for the different values of k_{bend} (Fig. 2 and S1A†). As can be observed in these figures, the radius of gyration decreases at low temperatures regardless of the stiffness of the copolymer chain, with a transition that becomes more marked as the chain stiffness increases. It is possible to identify a critical reduced temperature T_c at which the transitions occur, which also corresponds to a peak in the heat capacity as a function of reduced temperature (*vide infra*). The behaviour of the core density and the asphericity, however, depend critically on the stiffness of the polymer chain. While the core density for the fully flexible copolymer ($k_{bend} = 0$) exhibits a sharp increase at around the same temperature where the radius of gyration (R_g) decreases, for the stiffest copolymers ($k_{bend} = 10$) it stays constant around 0 for all temperatures. For intermediate values of k_{bend} ($k_{bend} = 3$) an increase in the core density and stabilization in two different values at low reduced temperatures is observed. Conversely, the asphericity shows a narrowing in the distribution of values for each reduced temperature as the temperature decreases, but the value at low temperatures depends on the chain stiffness, from 0.0 for $k_{bend} = 0$ to 0.25 for $k_{bend} = 10$. Interestingly, for intermediate stiffness ($k_{bend} = 3$) there are two distinct regions, around 0.1 and 0.5, to which the asphericity of the copolymer stabilizes at low temperatures (*vide infra* and S1B).

Fig. 3 depicts the contact maps for the copolymers for different values of chain stiffness (see also S2†). For a fully flexible copolymer ($k_{bend} = 0$), the first contacts formed (at high reduced temperatures) are preferentially between nearest neighbours (diagonal line), which at lower reduced temperatures change to contacts among all beads without a clear preference. With increasing chain stiffness, this pattern changes to the formation of next-neighbours contacts ($k_{bend} = 5$) that gets more marked at lower temperature, or the formation of contacts between opposite ends of the chain ($k_{bend} = 10$) that evolves into a preferred pattern of next-neighbours contacts as the reduced temperature decreases. This analysis shows that chain stiffness has a very strong effect on the secondary structure of the collapsed copolymers.

Downloaded by TECHNISCHE UNIVERSITEIT EINDHOVEN on 24 August 2012
Published on 22 June 2012 on http://pubs.rsc.org | doi:10.1039/C2SM25832C

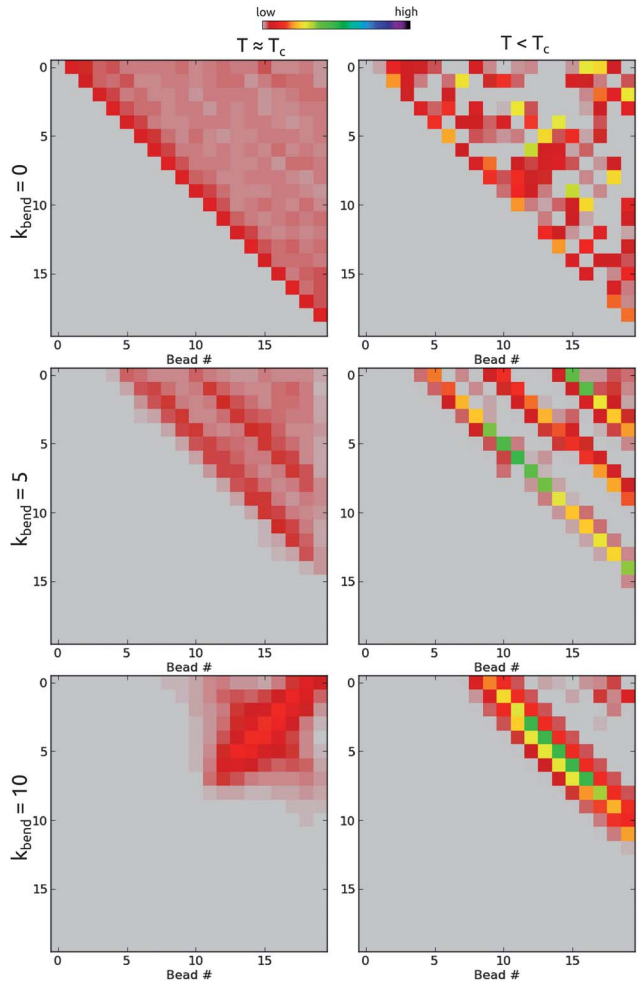

Fig. 3 Contact maps for B-type (directional) beads of AAAAB type copolymers at reduced temperatures at and below the T_c for selected values of k_{bend}. The scale bar on the top represents the fraction of sampled conformations at a given temperature that shows a specific contact. Only the top half of the symmetric heatmap is shown. Contact maps for other values of k_{bend} are given in S2†.

Combining the distributions of structural parameters as a function of temperature (Fig. 2) it is possible to define the most representative values of each property at a given temperature. This analysis allows for the discrimination of cases where the distribution is non-monomodal (*e.g.*, asphericity for $k_{bend} = 3$ at low temperatures, and for $k_{bend} = 10$ at $T \approx T_c$ Fig. 2 and *vide infra*) which would otherwise be overlooked if only temperature-averaged property values were considered. These values are evaluated at three reduced temperatures for each simulation; namely, at the temperature where the heat capacity has its first peak when cooling ($T \approx T_c$), and values higher ($T = 2.5$) and lower ($T = 0.5$) than T_c. Then, a second Wang–Landau simulation is performed for each value of k_{bend}, using the previously determined density of states as acceptance criteria to yield representative structures having the set of structural values as described above. The structures thus found (Fig. 4 and S3†) yield detailed insight into the distribution of the structural parameters and the contact maps as previously described. For example, the emergence of two different low-temperature structures for the semiflexible polymers results from the formation of either a more compact (asphericity ~0.1) or more extended (asphericity ~0.5) collapsed globule. At higher stiffness (*i.e.*, $k_{bend} \geq 5$) the patterns appearing in the contact maps are evidence of the formation of toroid-like structures. Furthermore, the contact map of the stiffest copolymer at a high temperature results from the preferential formation of hairpin structures, giving place to toroids at lower reduced temperature.

When comparing these representative structures with those found for homopolymer chains with all beads interacting with an isotropic potential (see ESI†), some differences are observed. Specifically, whereas some structural properties exhibit non-monomodal distributions in the copolymer, these are mostly monomodal in the homopolymer (see Fig. 2 and ESI†). For example, spherical as well as elongated collapsed structures are equally prevalent for $k_{bend} = 3$ in the copolymers, while almost only spherical ones are found in the homopolymer. Similarly, for $k_{bend} = 10$ elongated hairpin structures are found more frequently than toroidal structures in copolymer simulations around the T_c, whereas mostly toroids are found for the homopolymers.

From the final density of states obtained after the simulation, it is possible to calculate the heat capacity (C_v) of the system at all reduced temperatures. The heat capacities of a single homopolymer chain with beads interacting with an isotropic Lennard-Jones 12-6 nonbonded potential (Fig. 5, blue lines) yields results similar to what was found by Parsons and Williams[38] for a fully flexible polymer ($k_{bend} = 0$) and by Noguchi and Yoshikawa[65] for semiflexible and stiff polymers. In particular, the plots of the heat capacity *vs.* reduced temperature of the flexible polymers exhibit a broad peak and slowly increasing value of C_v as the reduced temperature decreases. With increasing chain stiffness (*i.e.*, higher k_{bend} values), this peak becomes sharper and the transition

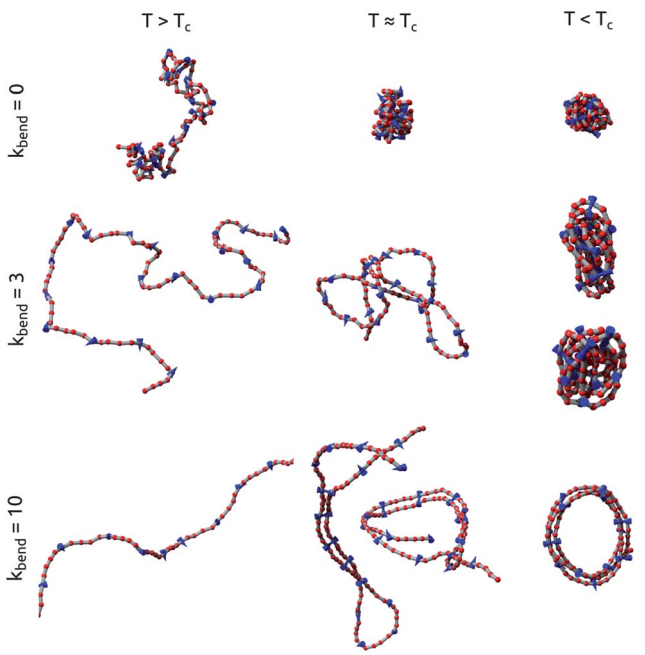

Fig. 4 Representative structures for the copolymer chains at different reduced temperatures and values of k_{bend}. Representative structures for other values of k_{bend} are given in S3†.

This journal is © The Royal Society of Chemistry 2012

Downloaded by TECHNISCHE UNIVERSITEIT EINDHOVEN on 24 August 2012
Published on 22 June 2012 on http://pubs.rsc.org | doi:10.1039/C2SM25832C

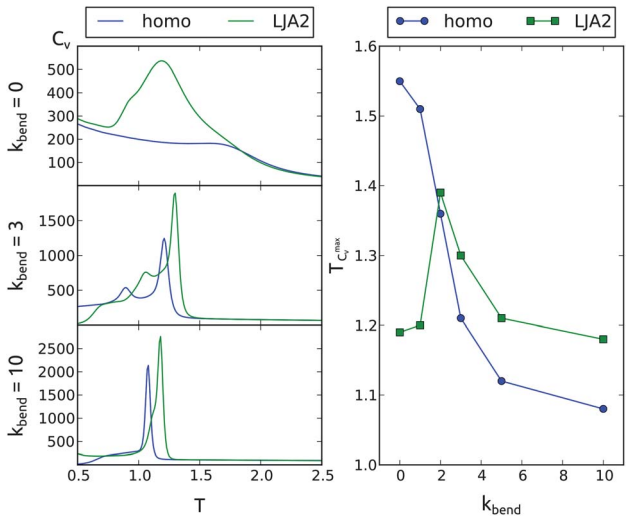

Fig. 5 Left: heat capacity as a function of reduced temperature of homopolymers composed of 100 A-type beads (blue) and copolymers having a directional B-type bead on every fifth position (green) on the chain for selected values of k_{bend}. Right: Temperature corresponding to the peak in the heat capacity plots for each value of k_{bend}; the lines serve as a guide to the eye.

temperature shifts to a lower reduced temperature. When every fifth bead of the sequence is made to interact *via* a directional potential, the transition becomes much sharper at all values of k_{bend}, and the temperature at which the heat capacity has a maximum is distinct from the simulation of the corresponding homopolymer at the same value of k_{bend} (Fig. 5, green lines). A plot of the location of this maximum as a function of the bending constant for both systems (Fig. 5, right) reveals an interesting trend: while the location of the peak is monotonously decreasing in the case of homopolymers, for the copolymers with directional beads there is a clear maximum around a value of $k_{bend} = 2$ or 3, with little change for the other values of k_{bend}. Comparing the heat capacity profiles, at low stiffness until about $k_{bend} = 2$ it is evident that the collapse of the chain is dominated by the interaction of backbone beads, as the heat capacities overlap for temperatures above the T_c of the homopolymer. At high stiffness, on the other hand, the T_c of the copolymer is clearly higher than that of the homopolymer. For these stiffer chains, it is the energy gain provided by dimer formation between directional beads that overcomes the penalty of bending the chain, leading to folding of the copolymer at a higher reduced temperature compared to the homopolymer.

Conclusions

Extensive Monte Carlo simulations of model copolymers have been presented, uncovering the critical role of flexibility and directional interactions on polymer collapse. The coarse-grained heteropolymers consist of a regular sequence of isotropically interacting LJ beads and beads interacting *via* a strong directional non-bonded potential, the latter representing the effect of hydrogen-bonding. Our simulations demonstrate that chain stiffness has a pronounced effect on the conformations of the collapsed structures as evidenced by the behaviour of various structural properties (*e.g.*, radius of gyration, core density and asphericity) during coil-to-globule collapse. Compared to a semi-flexible homopolymer in which beads interact *via* an isotropic potential only, the introduction of directional beads within the chain results in structural heterogeneity at temperatures around and below the critical temperature. Furthermore, this critical temperature for the coil-to-globule collapse transition of the heteropolymers as determined from the heat capacity profiles shows a non-intuitive dependence on the chain stiffness. This dependence can be rationalized by competing effects arising from the attraction between isotropic beads, which is dominant for flexible polymers, and the strong attraction between directional beads, which dominates the collapse of the stiffer heteropolymers.

Our results may be useful in the design of novel single-chain, polymeric nanoparticles consisting of regular copolymers in which one of the monomeric units has a strong, directional interaction.[28,29,32,66,67] To further explore the design space of these multiresponsive nanomaterials, future work will consider pseudo-random copolymer architectures, more detailed copolymer representations, and the effect of solvent on coil-to-globule collapse, as well as competition between intra- and intermolecular interactions in simulations of multiple heteropolymer chain architectures.

Acknowledgements

We wish to thank W. B. L. Gevers for his help in the implementation and understanding of the Wang–Landau algorithm and suggesting the modification by Swetnam and Allen.

Notes and references

1 M. Ouchi, T. Terashima and M. Sawamoto, *Chem. Rev.*, 2009, **109**, 4963–5050.
2 N. Badi and J.-F. Lutz, *Chem. Soc. Rev.*, 2009, **38**, 3383–3390.
3 B. M. Rosen and V. Percec, *Chem. Rev.*, 2009, **109**, 5069–5119.
4 K. Matyjaszewski and N. V. Tsarevsky, *Nat. Chem.*, 2009, **1**, 276–288.
5 R. K. Iha, K. L. Wooley, A. M. Nyström, D. J. Burke, M. J. Kade and C. J. Hawker, *Chem. Rev.*, 2009, **109**, 5620–5686.
6 M. Ouchi, N. Badi, J.-F. Lutz and M. Sawamoto, *Nat. Chem.*, 2011, **3**, 917–924.
7 J. M. Spruell and C. J. Hawker, *Chem. Sci.*, 2011, **2**, 18–26.
8 Y. Zhao, K. Thorkelsson, A. J. Mastroianni, T. Schilling, J. M. Luther, B. J. Rancatore, K. Matsunaga, H. Jinnai, Y. Wu, D. Poulsen, J. M. J. Frechet, A. P. Alivisatos and T. Xu, *Nat. Mater.*, 2009, **8**, 979–985.
9 Z. Sun, F. Bai, H. Wu, S. K. Schmitt, D. M. Boye and H. Fan, *J. Am. Chem. Soc.*, 2009, **131**, 13594–13595.
10 Y. Chen, M. Thorn, S. Christensen, C. Versek, A. Poe, R. C. Hayward, M. T. Tuominen and S. Thayumanavan, *Nat. Chem.*, 2010, **2**, 503–508.
11 R. J. Wojtecki, M. A. Meador and S. J. Rowan, *Nat. Mater.*, 2011, **10**, 14–27.
12 D. A. Christian, A. Tian, W. G. Ellenbroek, I. Levental, K. Rajagopal, P. A. Janmey, A. J. Liu, T. Baumgart and D. E. Discher, *Nat. Mater.*, 2009, **8**, 843–849.
13 T. Gadt, N. S. Ieong, G. Cambridge, M. A. Winnik and I. Manners, *Nat. Mater.*, 2009, **8**, 144–150.
14 E. A. Appel, J. Dyson, J. del Barrio, Z. Walsh and O. A. Scherman, *Angew. Chem., Int. Ed.*, 2012, **51**, 4185–4189.
15 H. Cabral, N. Nishiyama and K. Kataoka, *Acc. Chem. Res.*, 2011, **44**, 999–1008.
16 N. Nasongkla, E. Bey, J. Ren, H. Ai, C. Khemtong, J. S. Guthi, S.-F. Chin, A. D. Sherry, D. A. Boothman and J. Gao, *Nano Lett.*, 2006, **6**, 2427–2430.

View Online

17 T. Terashima, T. Mes, T. F. A. De Greef, M. A. J. Gillissen, P. Besenius, A. R. A. Palmans and E. W. Meijer, *J. Am. Chem. Soc.*, 2011, **133**, 4742–4745.
18 C. Tang, E. M. Lennon, G. H. Fredrickson, E. J. Kramer and C. J. Hawker, *Science*, 2008, **322**, 429–432.
19 T. Xu, N. Zhao, F. Ren, R. Hourani, M. T. Lee, J. Y. Shu, S. Mao and B. A. Helms, *ACS Nano*, 2011, **5**, 1376–1384.
20 G. Srinivas, D. E. Discher and M. L. Klein, *Nat. Mater.*, 2004, **3**, 638–644.
21 C. Peter and K. Kremer, *Soft Matter*, 2009, **5**, 4357–4366.
22 S. N. Fejer, D. Chakrabarti and D. J. Wales, *Soft Matter*, 2011, **7**, 3553–3564.
23 A. J. Williamson, A. W. Wilber, J. P. K. Doye and A. A. Louis, *Soft Matter*, 2011, **7**, 3423–3431.
24 S. Toksoz, H. Acar and M. O. Guler, *Soft Matter*, 2010, **6**, 5839–5849.
25 S. Whitelam, E. H. Feng, M. F. Hagan and P. L. Geissler, *Soft Matter*, 2009, **5**, 1251–1262.
26 T. E. Ouldridge, A. A. Louis and J. P. K. Doye, *Phys. Rev. Lett.*, 2010, **104**, 178101.
27 F. Yan, C. A. Hixson and D. J. Earl, *Phys. Rev. Lett.*, 2008, **101**, 157801.
28 E. J. Foster, E. B. Berda and E. W. Meijer, *J. Am. Chem. Soc.*, 2009, **131**, 6964–6966.
29 E. B. Berda, E. J. Foster and E. W. Meijer, *Macromolecules*, 2010, **43**, 1430–1437.
30 T. Mes, R. van der Weegen, A. R. A. Palmans and E. W. Meijer, *Angew. Chem., Int. Ed.*, 2011, **50**, 5085–5089.
31 E. Harth, B. V. Horn, V. Y. Lee, D. S. Germack, C. P. Gonzales, R. D. Miller and C. J. Hawker, *J. Am. Chem. Soc.*, 2002, **124**, 8653–8660.
32 M. Seo, B. J. Beck, J. M. J. Paulusse, C. J. Hawker and S. Y. Kim, *Macromolecules*, 2008, **41**, 6413–6418.
33 J. B. Beck, K. L. Killops, T. Kang, K. Sivanandan, A. Bayles, M. E. Mackay, K. L. Wooley and C. J. Hawker, *Macromolecules*, 2009, **42**, 5629–5635.
34 B. V. K. J. Schmidt, N. Fechler, J. Falkenhagen and J.-F. Lutz, *Nat. Chem.*, 2011, **3**, 234–238.
35 G. Zhang, F. M. Winnik and C. Wu, *Phys. Rev. Lett.*, 2003, **90**, 035506.
36 B. S. Murray and D. A. Fulton, *Macromolecules*, 2011, **44**, 7242–7252.
37 G. D. Rose, P. J. Fleming, J. R. Banavar and A. Maritan, *Proc. Natl. Acad. Sci. U. S. A.*, 2006, **103**, 16623–16633.
38 D. F. Parsons and D. R. M. Williams, *Phys. Rev. E: Stat., Nonlinear, Soft Matter Phys.*, 2006, **74**, 041804.
39 M. P. Taylor, W. Paul and K. Binder, *Phys. Rev. E: Stat., Nonlinear, Soft Matter Phys.*, 2009, **79**, 050801.
40 Y. Zhou, C. K. Hall and M. Karplus, *Phys. Rev. Lett.*, 1996, **77**, 2822.
41 A. Montesi, M. Pasquali and F. C. MacKintosh, *Phys. Rev. E: Stat., Nonlinear, Soft Matter Phys.*, 2004, **69**, 021916.
42 C. Forrey, J. F. Douglas and M. K. Gilson, *Soft Matter*, 2012, **8**, 6385–6392.
43 J. Borg, M. H. Jensen, K. Sneppen and G. Tiana, *Phys. Rev. Lett.*, 2001, **86**, 1031.
44 A. Trovato, J. Ferkinghoff-Borg and M. H. Jensen, *Phys. Rev. E: Stat. Phys., Plasmas, Fluids, Relat. Interdiscip. Top.*, 2003, **67**, 021805.
45 M. V. Athawale, G. Goel, T. Ghosh, T. M. Truskett and S. Garde, *Proc. Natl. Acad. Sci. U. S. A.*, 2007, **104**, 733–738.
46 A. R. Khokhlov and P. G. Khalatur, *Phys. Rev. Lett.*, 1999, **82**, 3456–3459.
47 A. K. Dasmahapatra, H. Nanavati and G. Kumaraswamy, *J. Chem. Phys.*, 2007, **127**, 234901.
48 S. Schnabel, M. Bachmann and W. Janke, *Phys. Rev. Lett.*, 2007, **98**, 048103.
49 S. N. Jamadagni, C. Bosoy and S. Garde, *J. Phys. Chem. B*, 2010, **114**, 13282–13288.
50 H. S. Ashbaugh and H. W. Hatch, *J. Am. Chem. Soc.*, 2008, **130**, 9536–9542.
51 C. Clementi, A. Maritan and J. R. Banavar, *Phys. Rev. Lett.*, 1998, **81**, 3287–3290.
52 R. Taylor and O. Kennard, *Acc. Chem. Res.*, 1984, **17**, 320–326.
53 F. Wang and D. P. Landau, *Phys. Rev. Lett.*, 2001, **86**, 2050–2053.
54 D. P. Landau, S.-H. Tsai and M. Exler, *Am. J. Phys.*, 2004, **72**, 1294–1302.
55 H. R. Warner, *Ind. Eng. Chem. Fundam.*, 1972, **11**, 379–387.
56 A. Milchev, A. Bhattacharya and K. Binder, *Macromolecules*, 2001, **34**, 1881–1893.
57 B. A. H. Huisman, P. G. Bolhuis and A. Fasolino, *Phys. Rev. Lett.*, 2008, **100**, 188301.
58 M. S. Shell, P. G. Debenedetti and A. Z. Panagiotopoulos, *Phys. Rev. E: Stat. Phys., Plasmas, Fluids, Relat. Interdiscip. Top.*, 2002, **66**, 056703.
59 N. Rathore, T. A. Knotts and J. J. de Pablo, *J. Chem. Phys.*, 2003, **118**, 4285.
60 A. D. Swetnam and M. P. Allen, *J. Comput. Chem.*, 2011, **32**, 816–821.
61 N. Metropolis, A. W. Rosenbluth, M. N. Rosenbluth, A. H. Teller and E. Teller, *J. Chem. Phys.*, 1953, **21**, 1087–1092.
62 A. Baumgärtner and K. Binder, *J. Chem. Phys.*, 1979, **71**, 2541.
63 N. Madras and A. D. Sokal, *J. Stat. Phys.*, 1988, **50**, 109–186.
64 F. T. Wall and F. Mandel, *J. Chem. Phys.*, 1975, **63**, 4592.
65 H. Noguchi and K. Yoshikawa, *J. Chem. Phys.*, 1998, **109**, 5070.
66 K. P. Nair, V. Breedveld and M. Weck, *Macromolecules*, 2011, **44**, 3346–3357.
67 J. M. Pollino and M. Weck, *Chem. Soc. Rev.*, 2005, **34**, 193–207.

Published on 22 June 2012 on http://pubs.rsc.org | doi:10.1039/C2SM25832C
Downloaded by TECHNISCHE UNIVERSITEIT EINDHOVEN on 24 August 2012

 This journal is © The Royal Society of Chemistry 2012

Addition and correction

View Online

Note from RSC Publishing

This article was originally published with incorrect page numbers. This is the corrected, final version.

The Royal Society of Chemistry apologises for these errors and any consequent inconvenience to authors and readers.

Downloaded by TECHNISCHE UNIVERSITEIT EINDHOVEN on 24 August 2012
Published on 22 June 2012 on http://pubs.rsc.org | doi:10.1039/C2SM25832C